European Journal of Mechanics B/Fluids 28 (2009) 532–540

Contents lists available at ScienceDirect

European Journal of Mechanics B/Fluids

www.elsevier.com/locate/ejmflu

Oblique roll instability in inclined buoyancy layers

J. Tao [a,*], F.H. Busse [b]

[a] LTCS and CAPT, Department of Mechanics and Aerospace Engineering, College of Engineering, Peking University, Beijing 100871, PR China
[b] Institute of Physics, University of Bayreuth, Bayreuth 95440, Germany

ARTICLE INFO

Article history:
Received 14 December 2007
Received in revised form 1 December 2008
Accepted 20 January 2009
Available online 23 January 2009

PACS:
47.55.P-
47.20.Ft

Keywords:
Boundary layer
Thermal convection
Shear instability
TS wave
Longitudinal roll
Oblique roll

ABSTRACT

When an inclined plate is heated in a stably stratified fluid, a buoyancy-driven boundary-layer flow will be generated. According to previous studies, such a layer is mainly subjected to two instability mechanisms: the transverse traveling (TS) waves and the stationary longitudinal (SL) rolls. In present paper we identify a novel oblique roll (OR) instability. The oblique rolls are more unstable than SL rolls in fluids with Prandtl numbers P of the order unity or less for all angles of inclination χ with respect to the horizontal except those close to 0°. The OR mode has smaller critical Grashof numbers than the TS waves in some regions of the $P-\chi$-parameter space. This feature is surprising because the transverse TS wave has been reported as the most unstable infinitesimal disturbances in boundary-layer flows. In comparison with TS waves, oblique rolls have a lower critical frequency, which coincides with the Brunt–Väisälä frequency of internal waves when the surface temperature is fixed and the tilt angle is large. Another important feature of the OR mode is that its amplitude decreases less rapidly with distance from the plate than the amplitudes of SL rolls and TS waves. As a result, OR mode disturbances penetrate into the stably stratified region for nearly three times the thickness of the boundary layer. Further investigation reveals that in low Prandtl number fluids with a uniform-heat-flux boundary the preference for onset of oblique rolls instead of TS waves is even stronger than in the case of a fixed temperature at the plate.

1. Introduction

Because of the relative simplicity of its transition to turbulence, thermal convection in an inclined fluid layer has received considerable attention as a hydrodynamic system in the past decades [1–4]. For convection between two inclined parallel plates with different fixed temperatures, it has been found that the streamwise longitudinal rolls represent the preferred form of convection at onset for a wide range of parameters. They may be transformed into wavy rolls by the wavy instability and in turn become transversely drifting wavy rolls as the Rayleigh number is increased further [5]. Another case of inclined layer convection is provided by the thermal boundary layer on an inclined heated plate, which is immersed in a thermally stratified fluid. The inclined buoyancy layer is of special interest to atmospheric scientists. Prandtl [6] first introduced this model for the analysis of valley and mountain winds. In his study he assumed a homogeneous boundary layer and derived a plane parallel flow solution with a reversal of its velocity profile in its outer part. While the meteorological literature has focused on daily and seasonal variations and the effects of actual topographies on the mountain-valley winds, for a review we refer to the book by Stull [7], we are interested in this paper in the stability of the basic solution of Prandtl [6]. Gill and Davey [8] investigated the linear stability of such buoyancy layer at a vertical wall, and the inclined case was first analyzed by Iyer [9]. He studied two types of instabilities: the transverse (streamwise periodic) traveling waves or TS waves and the longitudinal (spanwise periodic) rolls. Theoretical and numerical studies of Prandtl's buoyancy layer have made substantial progress [10–15], but mostly only transverse TS waves have been studied. Here we return to this subject in order to extend the stability analysis and to identify the most unstable modes. The paper starts with the mathematical formulation of the problem in Section 2, where the linear analysis method used in this paper is also discussed. The critical properties of longitudinal rolls, transverse traveling waves and oblique rolls are presented in Section 3 for the case of fixed temperature at the plate. In Section 4 results for the plate with fixed heating are described. Concluding remarks and an outlook on further work are offered in Section 5.

2. Mathematical formulation

We consider the Prandtl buoyancy layer which is inclined at an angle χ with respect to the horizontal as shown in Fig. 1. The temperature in the ambient fluid $T^*_\infty(s^*)$ varies linearly in the vertical direction, $T^*_\infty(s^*) = T^*_\infty(0) + N^*_\infty s^*$ where s^* is measured vertically opposite to the direction of gravity g. N^*_∞ is the temperature gradient in the medium. The wall temperature is raised by a fixed amount ΔT^* above that of the fluid outside the boundary layer.

* Corresponding author.
E-mail addresses: jjtao@pku.edu.cn (J. Tao), busse@uni-bayreuth.de (F.H. Busse).

0997-7546/$ – see front matter
doi:10.1016/j.euromechflu.2009.01.002

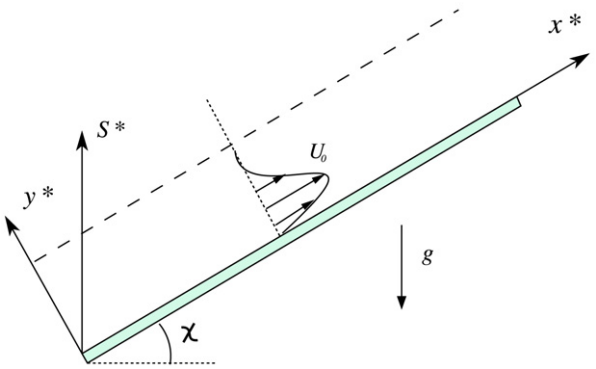

Fig. 1. Schematic geometry of an inclined buoyancy layer.

The coordinates x^* and y^* are parallel and normal to the wall respectively, and z^* points in the spanwise direction. The subscript '∞' and the hyperscript $*$ denote the ambient condition and dimensional quantities, respectively.

The governing equations in the Boussinesq approximation are given by

$$\begin{cases} \dfrac{\partial \mathbf{V}^*}{\partial \tau^*} + \mathbf{V}^* \cdot \nabla \mathbf{V}^* = -\nabla(P^*/\rho_r) - \mathbf{g}\gamma(T^* - T^*_\infty) + \nu \nabla^2 \mathbf{V}^*, \\ \dfrac{\partial T^*}{\partial \tau^*} + \mathbf{V}^* \cdot \nabla T^* = \kappa \nabla^2 T^*, \\ \nabla \cdot \mathbf{V}^* = 0, \end{cases} \tag{1}$$

where ρ_r, ν, κ and γ are the reference fluid density corresponding to $T^*_\infty(0)$, the kinematic viscosity, the thermal diffusivity and the coefficient of thermal expansion. In the following we shall use dimensionless length, time and temperature as defined by

$$(X, Y, Z) = \frac{(x^*, y^*, z^*)}{d}, \qquad \tau = \frac{\tau^* \nu}{d^2},$$

$$T = \frac{T^* - T^*_\infty}{\Delta T^*}, \qquad d = \left(\frac{4\nu\kappa}{g\gamma \sin^2(\chi) N^*_\infty} \right)^{1/4}.$$

The nondimensional parameters of the problem are the Grashof number and the Prandtl number,

$$G = \frac{g\gamma \sin(\chi) \Delta T^* d^3}{\nu^2}, \qquad P = \frac{\nu}{\kappa}.$$

The nondimensional variables are $U = U_0 + u$, $V = V_0 + v$, $W = w$ and $T = \theta_0 + \theta$, where u, v, θ, w are perturbations and U_0, V_0 and θ_0 constitute the undisturbed basic flow solution. Prandtl [6] found that the basic flow is parallel and that the velocity and the temperature profile as functions of the distance from the boundary are given by:

$$U_0 = \frac{G}{2} e^{-Y} \sin(Y), \qquad V_0 = 0, \qquad \theta_0 = e^{-Y} \cos(Y). \tag{2}$$

Since the density in the ambient fluid varies linearly in the vertical direction the Brunt–Väisälä frequency is given by $N_B = [-(g/\rho_r)(d\rho/ds^*)]^{1/2} = (g\gamma N_\infty)^{1/2}$. In dimensionless form the Brunt–Väisälä frequency becomes $N = \frac{2}{\sin(\chi)} P^{-1/2}$.

In the following stability analysis, general infinitesimal disturbances in the form of oblique rolls are represented by

$$\begin{Bmatrix} u \\ v \\ w \\ \theta \end{Bmatrix} = \begin{Bmatrix} \frac{i\alpha}{k^2} \Phi'(Y) + \Psi(Y) \\ \Phi(Y) \\ \frac{i\beta}{k^2} \Phi'(Y) - \frac{\alpha}{\beta} \Psi(Y) \\ \Theta(Y) \end{Bmatrix} e^{i(\alpha X + \beta Z - \omega \tau)}, \tag{3}$$

where $k^2 = \alpha^2 + \beta^2$. The following equations govern the stability of the basic state (2),

$$\begin{cases} \dfrac{\beta^2}{k^2} U_0' \Phi + (i\alpha U_0 - i\omega)\Psi = \Psi'' - k^2 \Psi + G \dfrac{\beta^2}{k^2} \Theta, \\ \big(\Phi'' - k^2 \Phi\big)(i\alpha U_0 - i\omega) - i\alpha U_0'' \Phi \\ \quad = \Phi'''' - 2k^2 \Phi'' + k^4 \Phi - i\alpha G \Theta' - k^2 G \operatorname{ctg} \chi \, \Theta, \\ \Theta'' - k^2 \Theta - i(\alpha U_0 - \omega) P \Theta = \dfrac{4}{G} \left(\dfrac{i\alpha}{k^2} \Phi' + \Psi + \operatorname{ctg} \chi \, \Phi \right) + P \theta_0' \Phi \end{cases} \tag{4}$$

with the boundary conditions

$$\begin{aligned} \Psi(0) = \Phi'(0) = \Phi(0) = \Theta(0) = \Psi(\infty) \\ = \Phi'(\infty) = \Phi(\infty) = \Theta(\infty) = 0, \end{aligned} \tag{5}$$

where the prime $'$ indicates d/dY. α and β assume real positive values. The onset of the instability occurs at the lowest value of the Grashof number G for which a real frequency ω can be obtained. Traveling (TS) waves and longitudinal rolls correspond to vanishing β and α, respectively. At the end of Section 3, the effect of uniform-heat-flux boundary condition on the unstable modes will be discussed, and $\Theta'(0) = 0$ will be used in conditions (5) instead of $\Theta(0) = 0$. The stability problem (4) and (5) constitutes a eighth-order differential equation with eight boundary conditions, which is solved with the same method as used by Iyer [9]. When Y is very large the four linearly independent solutions behave as $e^{\lambda_j Y}$ with $j = 1, 2, 3, 4$. The λ_j are the complex roots with negative real parts of the asymptotic form of the governing equation,

$$\begin{aligned} &\left[\big(\lambda^2 - k^2 + i\omega P\big)\big(\lambda^2 - k^2 + i\omega\big) + 4\frac{\beta^2}{k^2} \right] \big(\lambda^2 - k^2 + i\omega\big)\big(\lambda^2 - k^2\big) \\ &\quad = \big(\lambda^2 - k^2 + i\omega\big) \left[4k^2 \operatorname{ctg}^2 \chi + i8\alpha\lambda \operatorname{ctg} \chi - \frac{4\alpha^2}{k^2} \lambda^2 \right]. \end{aligned} \tag{6}$$

The disturbance governing equations are integrated with a fourth-order Runge–Kutta method marching in from a large value of Y to the wall. A value of $Y_{\max}$ of 20 was found to be sufficiently large for all unstable modes discussed in this paper. For fixed values of wavenumber α, β, tilt angle and Prandtl number, G and ω are obtained by a shooting method to guarantee that the nonzero linear solutions corresponding to λ_js can be combined at the wall to satisfy the boundary conditions (5). For details of the solving method, we refer to the previous paper [9].

3. Results for the plate with fixed temperature

The effects of the tilt angle and of the Prandtl number on the instability in the form of transverse traveling (TS) waves and longitudinal rolls have been studied by Iyer [9] for $P \leqslant 1$, and it was concluded that the TS wave is the most unstable mode. We have confirmed the data of his linear analysis and have found some new features. First, it turns out that the Grashof number for the onset of stationary longitudinal (SL) rolls with zero frequency does not correspond to a local minimum, but to a saddle point in the α, β-plane for nearly the entire parameter space investigated in [9]. An example of this saddle is illustrated in Fig. 2(b) for $P = 0.72$ and $\chi = 55°$. Since higher Grashof numbers G of neutral states represents more stable modes, which are of lesser interest, only the regimes with small G are shown in Fig. 2. The descent from the saddle point always leads to a minimum of G with $\beta = 0$, which corresponds to the transverse traveling (TS) wave. In the case of Fig. 2 this minimum with $G = 136.4$ is shown in Fig. 2(a). Second, by browsing the α, β-plane we find another minimum of G as shown in Fig. 2(c) which corresponds to the most unstable oblique mode and will be referred to by OR in the following. The critical parameters are $G = 120.22$, $\alpha = 0.042$, $\beta = 0.463$ and $\omega = 2.942$, respectively. Since α is about one order smaller than β,

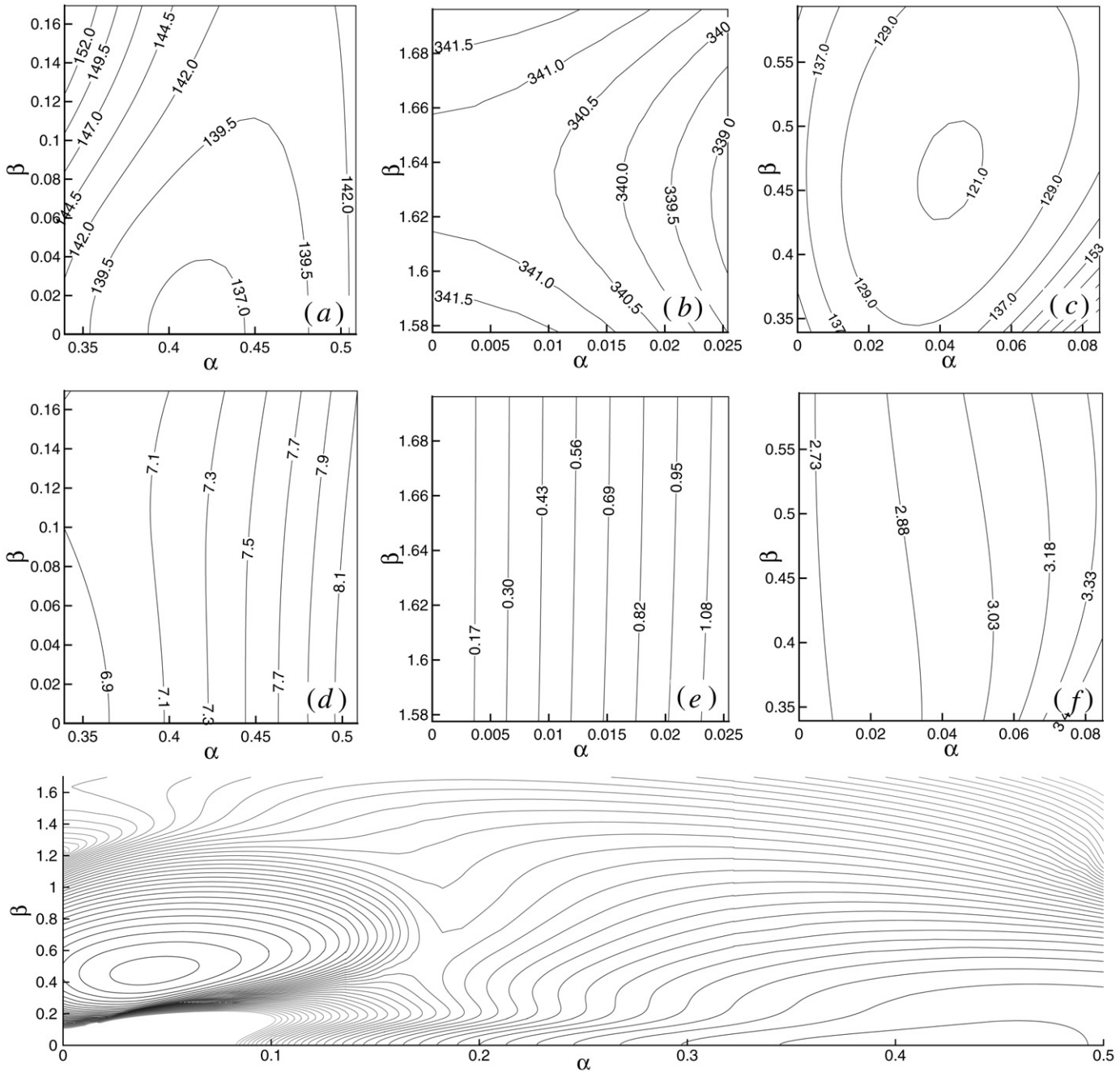

Fig. 2. Iso-contours of the G (top row) and the corresponding frequencies ω (middle row) of neural states for $P = 0.72$ and $\chi = 55°$. A global plot with isolines of G is shown at bottom. Darker contour represents smaller G. Since modes with larger G are more stable and of lesser interest, the contours in the region of higher G is not shown.

such an oblique roll is nearly aligned with the streamwise direction. The most surprising result illustrated in Fig. 2 is that the oblique roll has an even smaller critical Grashof number than the transverse traveling wave. It is well known for forced-convection boundary layer flows, that transverse TS waves are more unstable than any oblique mode in accordance with Squire's transformation [16]. The preference for oblique rolls in the present case does not contradict Squire's theorem [16] because of the buoyancy terms in Eqs. (4). Although a few cases in the vicinity of the neutral states of transverse TS waves and longitudinal rolls were analyzed in [9], the most unstable OR mode was not found in that study.

It should be noted that there is a full symmetry of the solution Φ, Ψ and Θ in $\pm\beta$, and that is why the iso-contours of marginal G cross the α-axis at right angles (bottom plot of Fig. 2). It can be verified easily with Eq. (4) that for any solution with α, ω and β, there is also a solution with the same marginal G with $-\alpha, -\omega$ and β, but this solution differs in that its imaginary parts have the opposite sign. Once the sign of ω has been fixed there is no symmetry in G values of $\pm\alpha$. That is why the iso-contours of G do not usually cross the β-axis with a right angle.

The neutral curves for $\chi = 30°$, $P = 0.72$ and 2.5 are shown in Fig. 3. It is illustrated that the critical frequency of the TS wave is larger than that of the oblique roll mode, and the critical G and wavenumber of the OR mode and of the TS wave are less than those of the SL roll mode. It is also shown in Fig. 3 that for $P = 2.5$ the oblique roll mode has disappeared and the transverse TS wave is the most unstable mode. When the oblique roll becomes more unstable than the TS wave, the laminar-turbulence transition scenario should obviously be different from the classical

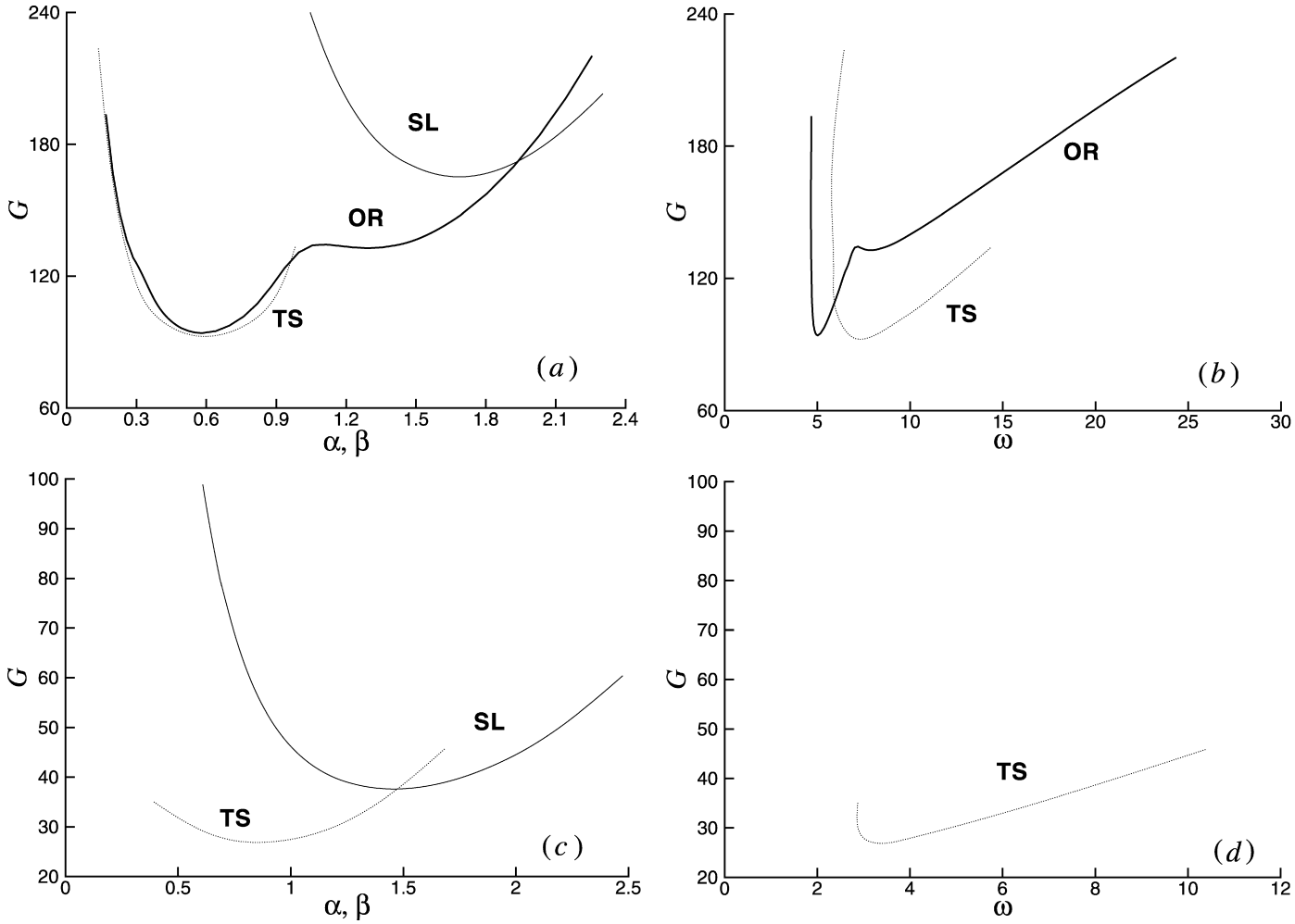

Fig. 3. The neutral curves in the $k - G$ planes (a)(c) and the $\omega - G$ planes (b)(d) for transverse traveling waves (TS), stationary longitudinal rolls (SL) and oblique rolls (OR) with $P = 0.72$ (top) and 2.5 (bottom) at $\chi = 30°$. For the oblique roll the abscissa measures $(\alpha^2 + \beta^2)^{1/2}$, where α and β keep the same ratio as at the critical point.

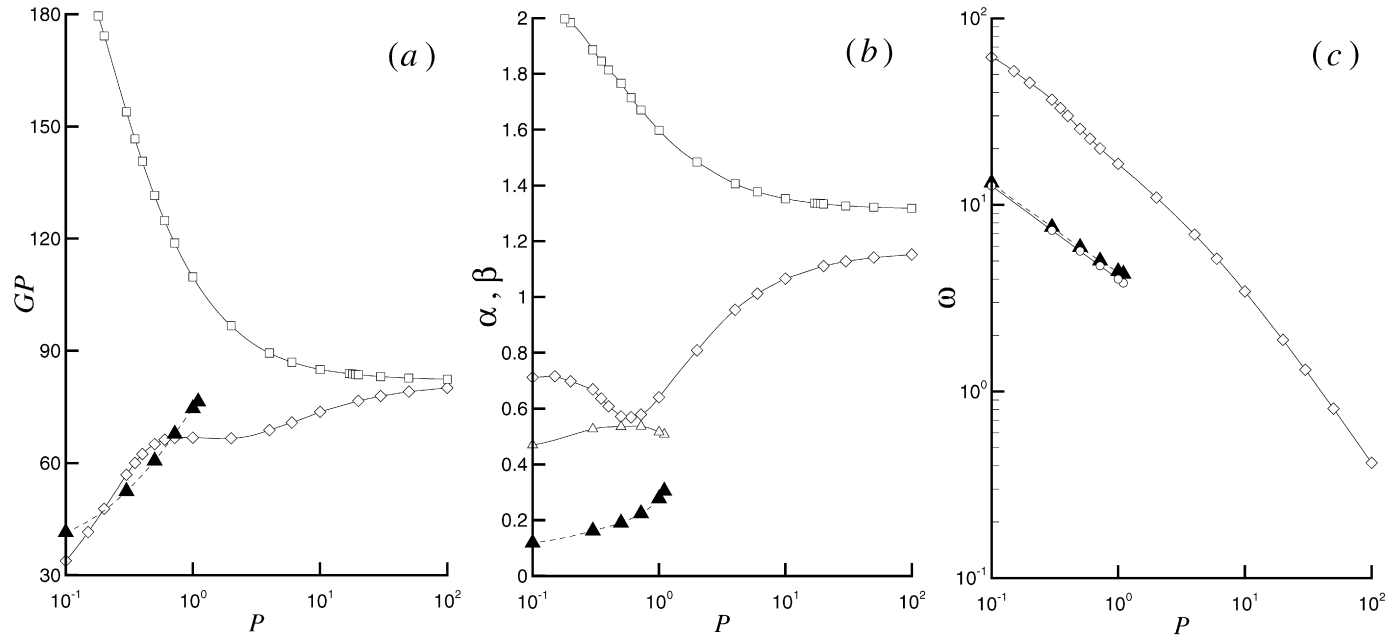

Fig. 4. The critical Grashof number G (a), wavenumber α, β (b) and frequency ω (c) as functions of the Prandtl number P at $\chi = 30°$ for TS waves (open diamonds), SL rolls (squares) and oblique rolls (triangle), respectively. The critical streamwise and spanwise wavenumbers α and β for oblique rolls are indicated by closed and open triangles in (b). The circles in (c) indicate the nondimensional Brunt–Väisälä frequency N at the critical state of the oblique roll mode.

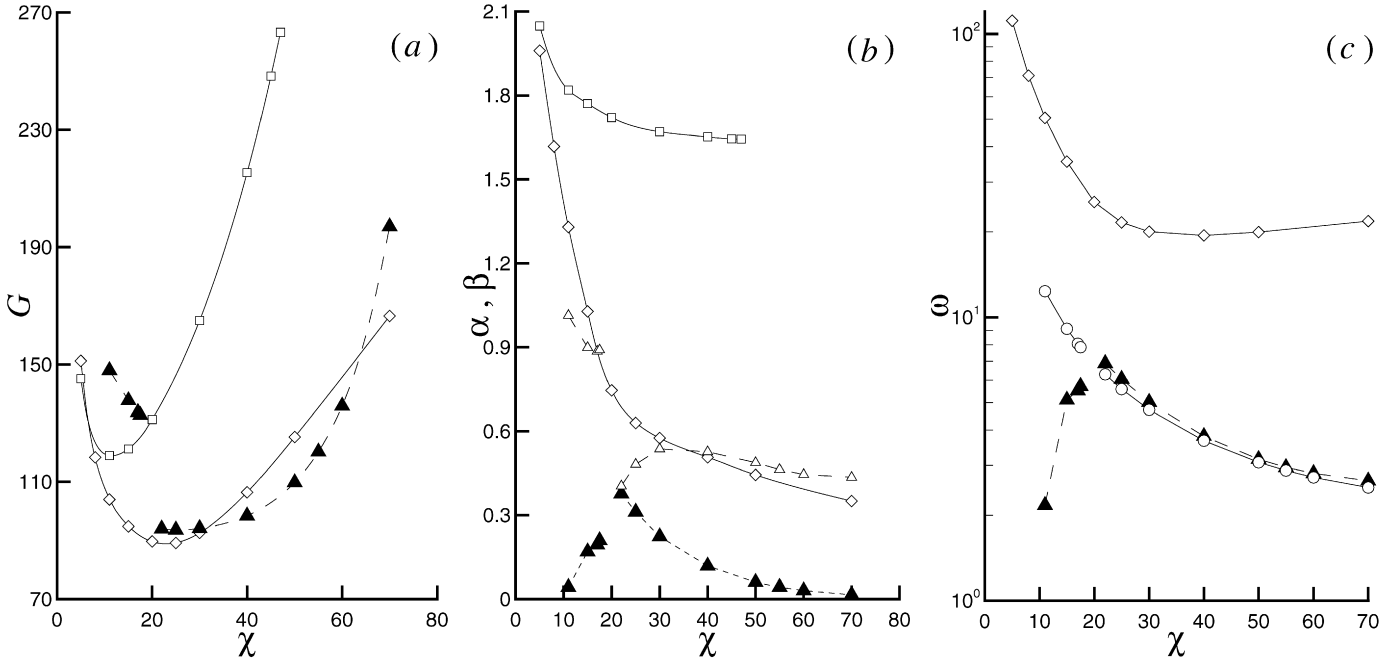

Fig. 5. The critical Grashof number G (a), wavenumber α, β (b) and frequency ω (c) as functions of χ for $P = 0.72$. Symbols represent the same modes as shown in Fig. 4.

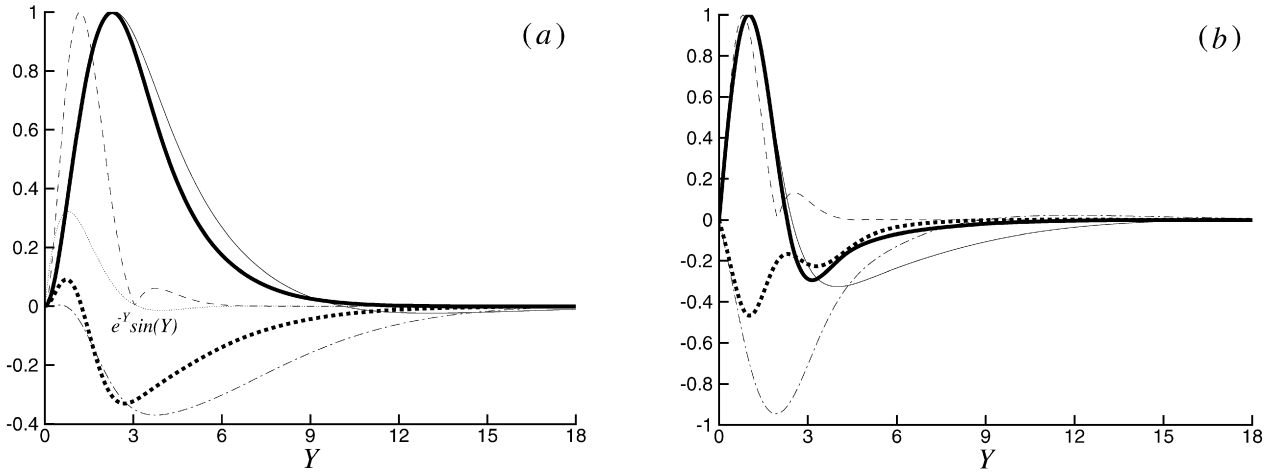

Fig. 6. Normalized amplitude profiles of the normal velocity Φ (a) and of the temperature Θ (b) as functions of normal distance Y for $P = 0.72$ and $\chi = 30°$ at the critical states. The dashed lines indicate the results $|\Phi|/|\Phi|_{\max}$ in (a) and $|\Theta|/|\Theta|_{\max}$ in (b) for the SL roll. The data $\Phi_r/\Phi_{r,\max}$, $\Phi_i/\Phi_{r,\max}$ in (a) and $\Theta_r/\Theta_{r,\max}$ and $\Theta_i/\Theta_{r,\max}$ in (b) are given by the thick solid line and the thick dotted line for the TS wave and by the thin solid line and the dash-dotted line for the oblique roll. The profile shape of the basic velocity (thin dotted line) $e^{-Y}\sin(Y)$ is also drawn in (a) as a reference.

one. Therefore, it is of interest to determine the parameter region where the oblique roll is the most unstable mode.

The dependence on the Prandtl number of the critical parameter values for SL rolls, oblique rolls and TS waves are shown in Fig. 4 for $\chi = 30°$. With increasing Prandtl number, the critical Grashof numbers of all three modes decrease. Among the three modes the SL roll has the largest critical wavenumber and the TS wave is characterized by the highest critical frequency. TS waves set in first except for $0.2 \lesssim P \lesssim 0.7$ where the oblique roll is the most unstable mode. For $P > 1.1$, the critical OR mode can no longer be found, and the critical Grashof numbers of TS waves and SL rolls draw increasingly closer with growing P. The TS wave persists as the most unstable mode, however.

The dependence on the tilt angle in the case $P = 0.72$ is shown in Fig. 5. Several instability exchanges are noteworthy. For $\chi \leqslant 5°$ SL rolls set in before the TS waves. This is reasonable because when the plate is almost horizontal, the problem becomes quite similar to Rayleigh–Bénard problem where convection rolls are the dominant pattern. This phenomenon has not been reported by Iyer [9] because he did not consider sufficiently small tilt angles χ. More importantly, when χ is between 30° and 64° the onset of oblique roll precedes that of the TS wave. As shown in Fig. 5(b), the streamwise wavenumber of the OR mode is smaller than its spanwise wavenumber such that the flow structure of the OR mode is a vortex roll nearly aligned with the streamwise direction. It is interesting to note that when $\chi > 22°$ (Fig. 5(c)), the critical frequency of the OR mode and the dimensionless Brunt–Väisälä frequency N coincide as the tilt angle χ (relative to the horizontal) increases. This suggests a strong connection between the origin of the oscillatory behavior of oblique roll and internal waves at large tilt angles. The effects on the frequency of the advection by the basic flow appear to be relatively small since the streamwise wavenumber α of the OR mode is rather small and the amplitude of the OR mode is quite high outside the boundary layer region where the

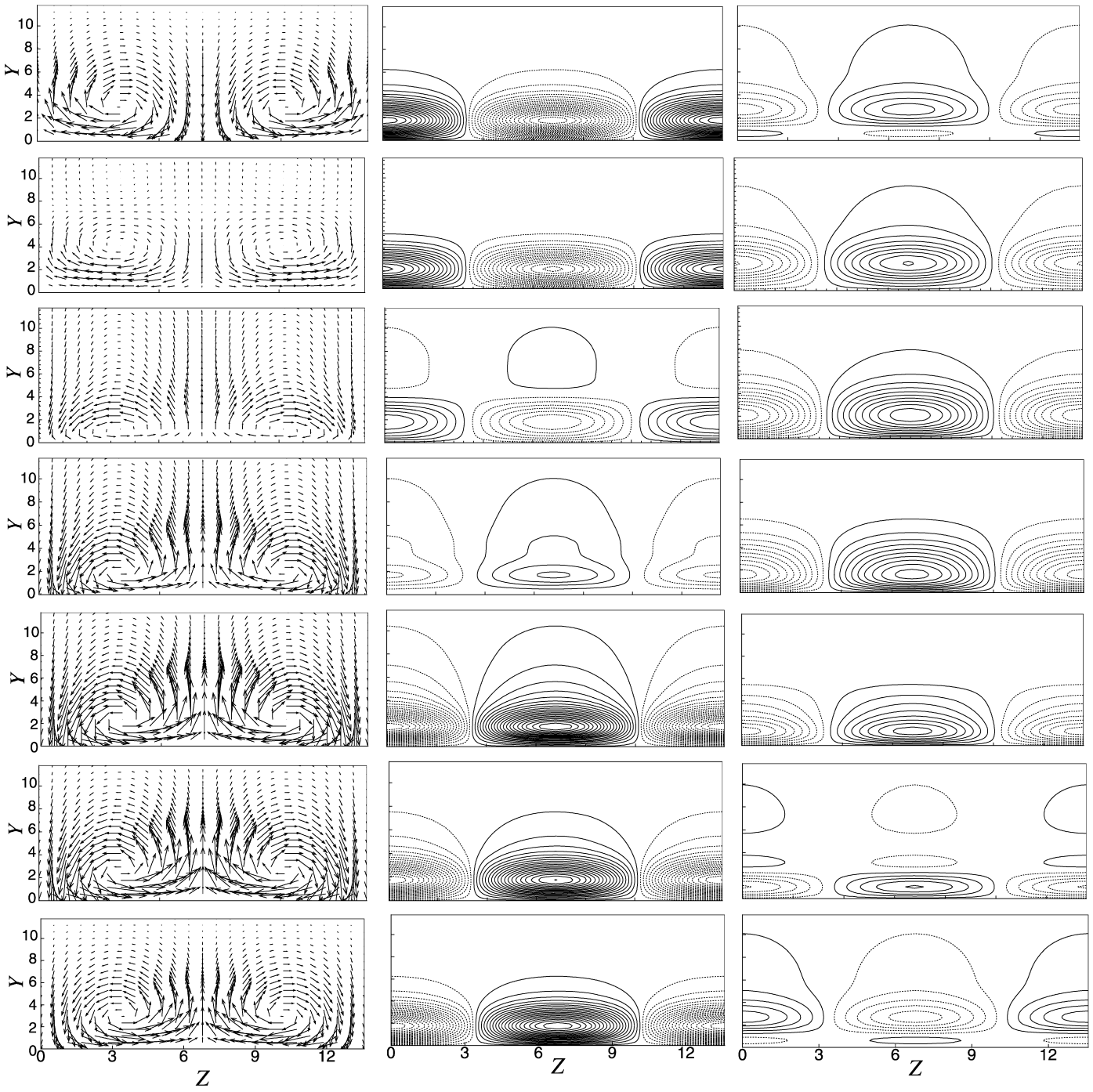

Fig. 7. Disturbing velocity in $Y-Z$ plane (left), contours of streamwise velocity u (middle) and temperature ϕ (right) of superposition of critical oblique rolls with $\pm\beta$ at $(G,\alpha,\beta,\omega)=(120.22, 0.042, 0.463, 2.942)$ for $P=0.72$ and $\chi=55°$. The figures from top to bottom are obtained at $X=0$ and $\tau=n\pi/6\omega$ with $n=0,1,\ldots,6$. Contours of negative values are dashed lines.

basic flow is concentrated. The minor importance of advection is also evident from the property that the frequency remains finite in the limit $\alpha\to 0$ as shown in Fig. 2(e).

When the tilt angle is small, the local minimum of G for the OR mode disappears around $\chi=21.5°$ and reappears for $\chi<17.5°$ with an oscillation frequency quite different from the Brunt–Väisälä frequency N. The OR mode obviously changes its character in this regime and its frequency now reflects its advection by the basic boundary layer flow. It is also illustrated in Fig. 5(c) that a further decrease of χ will decrease both the frequency and the streamwise wavenumber of the OR mode, and the oblique roll almost changes to another stationary longitudinal roll at $\chi=11°$. When the plate is almost horizontal ($\chi<10°$) the OR mode ceases to exist and the SL mode or the TS wave dominate the flow.

An unstable mode that does not correspond to a local minimum of G in the α,β-plane can usually not be physically realized. According to our calculations, the saddle point of the SL roll mode changes into a minimum of G at a nearly horizontal position of the plate, e.g. $\chi\leqslant 5°$ for $P=0.72$ (Fig. 5(a)) and for fluids of large Prandtl numbers, e.g. $P\geqslant 18$ at $\chi=30°$. We thus conclude that the most unstable mode of a buoyancy layers will be transverse TS waves, oblique rolls or stationary longitudinal rolls depending on the tilt angle and the Prandtl number.

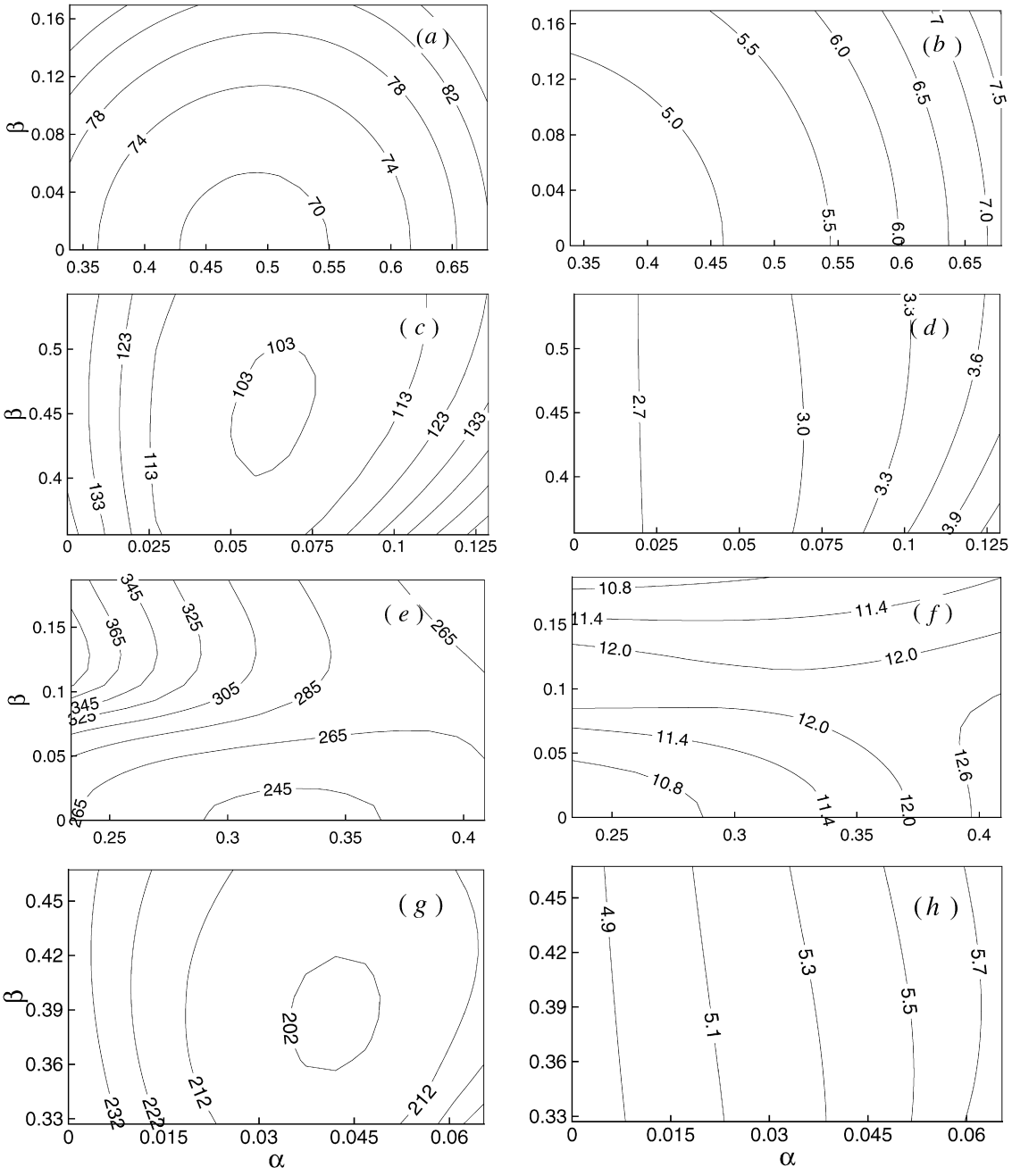

Fig. 8. Iso-contours of the G (left column) and the corresponding frequencies ω (right column) of neutral states at $\chi = 55°$ for $P = 0.72$ (a)–(d) and $P = 0.2$ (e)–(h) with the constant heat flux condition $\Theta'(0) = 0$.

Associated with the contrast between the wavenumbers of the three modes is a contrast between the dependences of their velocity and temperature fields on the Y-coordinate. Critically unstable modes are shown in Fig. 6. The critical parameters $(G, \alpha, \beta, \omega)$ for TS wave, oblique roll and SL roll are (92.6, 0.575, 0, 7.082), (94.16, 0.224, 0.536, 5.031) and (165.0, 0, 1.67, 0), respectively, at $P = 0.72$ and $\chi = 30°$. While the SL rolls are essentially confined to the buoyancy layer (roughly $Y \lessapprox 5$), the oblique rolls penetrate into the stably stratified medium nearly three times farther than the thickness of the buoyancy layer. This property means that the OR unstable mode has a stronger receptivity than other modes to far field disturbances. As shown in Figs. 4(c) and 5(c), the OR mode oscillates with almost the same frequency as the nondimensional Brunt–Väisälä frequency of internal waves in the stably stratified region.

Since only even powers of β appear in Eqs. (4) solutions with β and $-\beta$ and superpositions thereof are possible. A particular solution that is symmetric about planes $Z = n\pi/\beta$ offers some illuminating insights into the dynamics the OR-instability as shown in Fig. 7 where the variation through half a period is presented. The oscillation of the vortex manifests itself by an upward movement of the vortex and a subsequent decay in the far field. In the meantime the flow at the bottom of the buoyancy layer changes from inrush towards the plate to outward ejection or vice versa. Consequently, a new vortex with reversed circulation appears near the plate (Fig. 7 at $\tau = \pi/3\omega$). It grows and moves upwards and replaces the previous vortex finally after half a period. Simultaneously, strong high-low speed streaks are formed and change direction periodically (middle column of Fig. 7). Because of the periodicity, the flow patterns shown in Fig. 7 are the same as for the flow

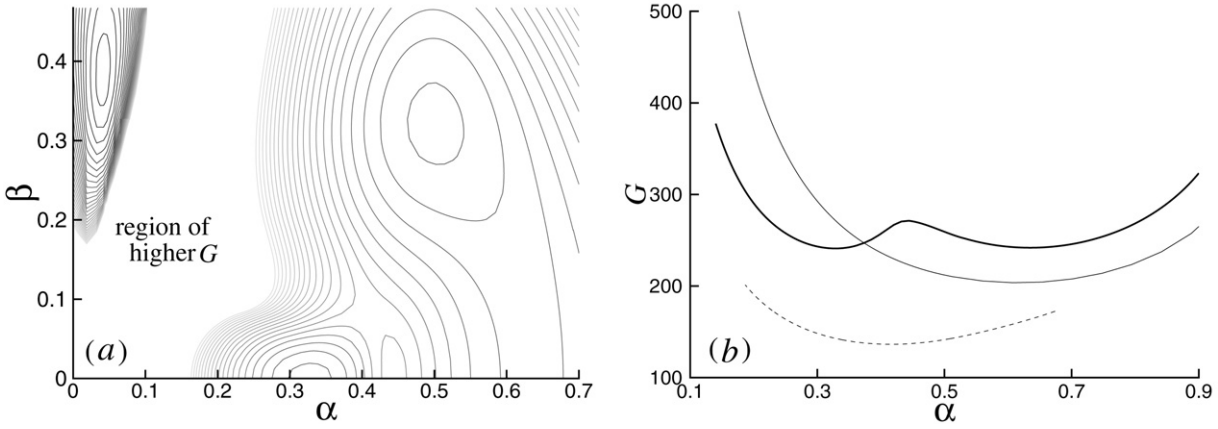

Fig. 9. (a) The G surface of neutral state for $P = 0.2$ with the thermal condition $\Theta'(0) = 0$ at $\chi = 55°$. Darker contour represents smaller G. (b) Neutral curves of TS waves at $\chi = 55°$. The thick solid and solid lines indicate the results of $P = 0.2$ for conditions $\Theta'(0) = 0$ and $\Theta(0) = 0$, respectively. The neutral curve of $P = 0.72$ with $\Theta(0) = 0$ condition is drawn with a dashed line for reference.

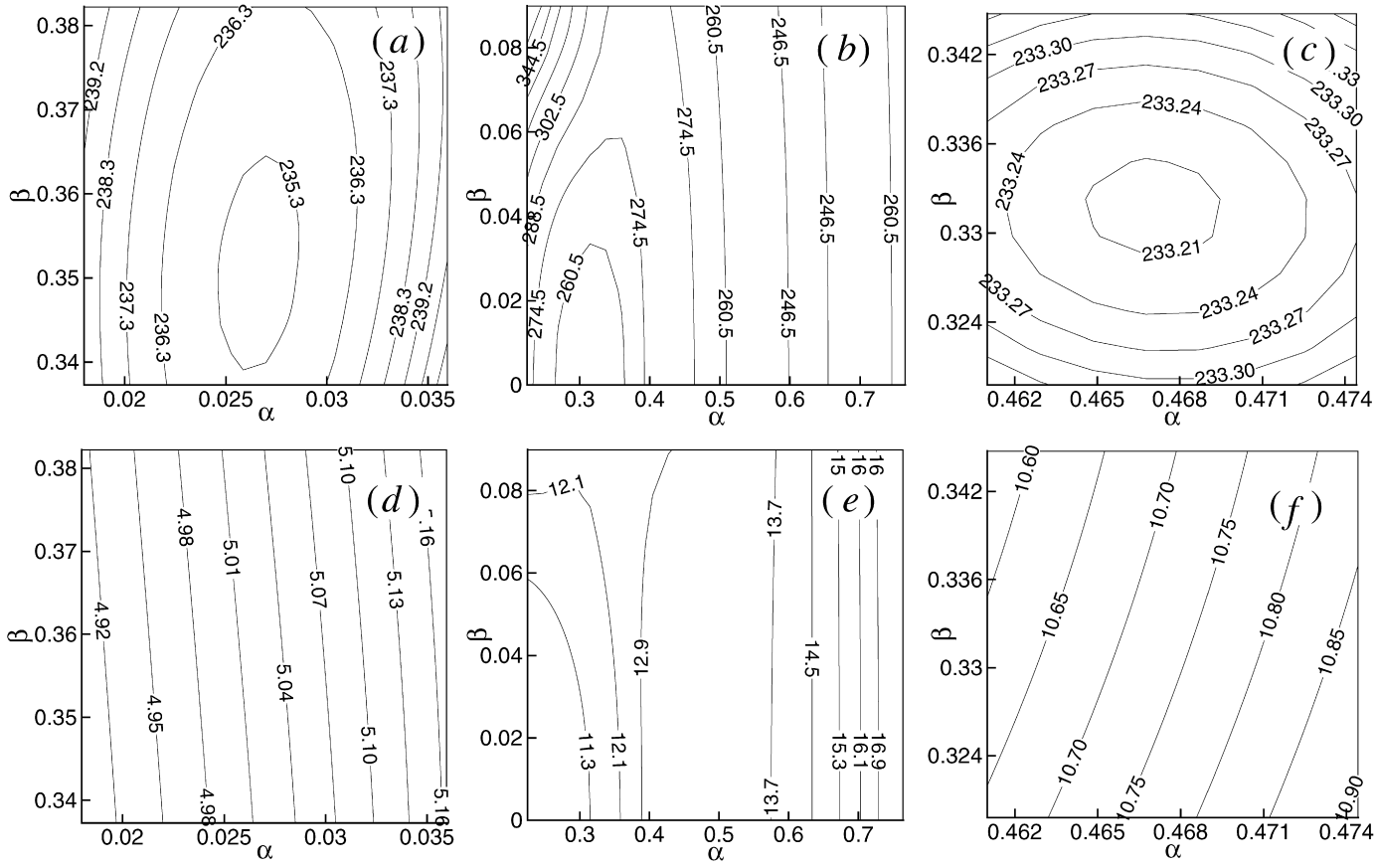

Fig. 10. Iso-contours of the G (top row) and the corresponding frequencies ω (bottom row) of neural states for $P = 0.2$ and $\chi = 62.2°$ with condition $\Theta'(0) = 0$.

at the fixed time $\tau = 0$ and $X = -n\pi/6\alpha$, $n = 0, 1, \ldots, 6$. Among the superpositions of left and right traveling waves the symmetric one displayed in Fig. 7 is only a particular one among a continuum. It offers the advantage that a dynamical process can be visualized in a simple way. It may also be preferred in experiments where the presence of side walls will usually cause reflections. At least it can be expected that oscillating pattern similar to that shown in Fig. 7 play an important role in the transition to turbulence.

4. Results for the plate with fixed heating

For a buoyancy layer on an inclined plate with the boundary condition of an uniform heat flux, the basic flow solution (2) is still applicable, and the disturbance equations (4) and (5) also remain unchanged except that the thermal boundary condition changes from $\Theta(0) = 0$ to $\Theta'(0) = 0$. Since the SL mode is usually not the most unstable mode, only the TS wave and OR modes are shown in Fig. 8. Comparing this figure with Fig. 2 one finds that the critical parameters $(G, \alpha, \beta, \omega)$ for the TS wave change from (136.4, 0.416, 0, 7.245) to (68.9, 0.485, 0, 5.107) for $P = 0.72$, and for $P = 0.2$ they change from (203.66, 0.608, 0, 11.492) to (241.17, 0.327, 0, 11.214). The iso-flux boundary condition thus destabilizes (stabilizes) the TS wave mode for $P = 0.72$ ($P = 0.2$) at $\chi = 55°$. This effect of the thermal boundary condition is similar to that in the case of a vertical plate [13].

As shown in Fig. 8 the values of the critical parameters $(G, \alpha, \beta, \omega)$ of the OR mode are (101.867, 0.0626, 0.45, 2.953) for $P = 0.72$ and (200.85, 0.042, 0.386, 5.364) for $P = 0.2$. The OR mode thus has a smaller critical G than the TS wave for $P = 0.2$, though TS waves are more unstable under the $\Theta(0) = 0$ condition, where the critical G for TS waves and OR modes are 203.66 and 285.69 at $\chi = 55°$, respectively. Similar to the cases with the $\Theta(0) = 0$ condition, the critical frequencies of the OR mode are close to the nondimensional Brunt–Väisälä frequencies 2.877 and 5.459 for $P = 0.72$ and 0.2, respectively. For iso-flux boundary condition the disturbance amplitude profiles of oblique rolls are similar to those shown in Fig. 6 except that instead of Θ_r and Θ_i, Θ_r' and Θ_i' vanish at the plate. Since the TS wave mode becomes stabilized with the change to the $\Theta'(0) = 0$ condition, we conclude that buoyancy layers with small Prandtl numbers usually prefer oblique rolls instead of TS waves as the most unstable mode.

The saddle point at the top-right corner of Fig. 8(e) leads to the possibility of another critical point of an oblique roll mode. A new minimum of G with the parameter values $(G, \alpha, \beta, \omega) = (232, 0.502, 0.327, 11.514)$ is found as shown in Fig. 9(a). The G-value is higher than the critical G shown in Fig. 8(g). The disturbance field of this new OR mode penetrates only by two times the thickness of the boundary layer into the stably stratified region which is much less than the penetration of the other OR mode. Another difference between these two oblique roll modes is that the new mode's frequency is higher than the value 5.459 of the internal wave, but close to the frequency 11.214 of the critical TS wave. As shown in Fig. 9(b) there are two minima on the neutral curve of the TS wave (thick solid line), and the minimum with larger streamwise wave number corresponds to a saddle point in the G-surface (Fig. 9(a)). The descent from this saddle point leads to the minimum of the new oblique roll mode.

In contrast to the case with the iso-flux boundary condition, the TS waves for $P = 0.2$ and $P = 0.72$ with the $\Theta(0) = 0$ condition have only one minimum on their neutral curves as shown in Fig. 9(b), and the new OR mode is not found in their corresponding G-surfaces. According to our calculations with the iso-flux boundary condition, this new OR mode exists only for $0.15 < P < 0.34$ at $\chi = 55°$, and becomes more and more important with the increase of the tilt angle for fluids of small P. For example, it becomes the most unstable mode for $\chi \geqslant 62.2°$ at $P = 0.2$. It is shown that the critical G of the new OR mode (Fig. 10(c)) and the previous OR mode (Fig. 10(a)) at $P = 0.2$ are 233.2 and 235.1, respectively. The critical frequency 5.02 of the previous oblique roll mode (Fig. 10(d)) is close to the internal wave frequency $N = 5.05$, while the critical frequency of the new OR mode is two times larger than N and is not far from the value of the critical TS wave as shown in Figs. 10(e) and 10(f). In addition, a comparison of Figs. 9 and 10(b) shows that the minimum value of G corresponding to the lower wavenumber α on the neutral curve of the TS wave begins to exceed the minimum with the larger value of α when the tilt angle χ increases from 55° to 62.2° for $P = 0.2$. The latter minimum at $\alpha = 0.63$ still corresponds to a saddle point in the α–β plane (Fig. 10b). For $P > 0.42$ the new OR mode disappears independently of the tilt angle. In future studies on low Prandtl number fluids the new oblique roll mode deserves to receive special attention.

5. Concluding discussion

In this paper the relationship between longitudinal rolls and transverse TS-waves in a tilted buoyancy layer immersed in a thermally stratified fluid has been clarified and a new instability in the form of oblique rolls (OR) has been identified. Several novel features of the OR-instability are likely to be important in the process of the transition to turbulence. First, since the oblique rolls are more unstable than TS waves at some tilt angles, the boundary-layer flow could be three-dimensional at the onset of instability. Second, at large tilt angles the background vertical thermal stratification may affect the buoyancy layer in that the oblique roll mode is traveling with the internal wave frequency. Third, because the OR-mode disturbance extends farther than the TS-waves in the Y-direction, oblique rolls are expected to have a stronger receptivity to far field disturbances than TS-waves.

It is hoped that this paper will stimulate experimental and numerical studies of the new instability which combines features of convection and internal waves. Since thermal boundary conditions in experiments usually lie between the $\Theta(0) = 0$ and $\Theta'(0) = 0$ conditions, the effect of the latter condition on the instabilities has also been investigated in this paper. The combination of the $+\beta$ and $-\beta$ solutions yields a streamwise vortex that just oscillates locally without traveling in the spanwise direction. This property should facilitate the observation of the OR-instability in future experiments.

Acknowledgements

This work has been supported by the National Natural Science Foundation of China (10672003). The partial support of the Alexander von Humboldt Foundation is gratefully acknowledged.

References

[1] J.E. Hart, Transition to a wavy vortex regime in convective flow between inclined plates, J. Fluid Mech. 48 (1971) 265–271.
[2] R.M. Clever, F.H. Busse, Stabilities of longitudinal convection rolls in an inclined layer, J. Fluid Mech. 81 (1977) 107–127.
[3] K.E. Daniels, B.B. Plapp, E. Bodenschatz, Pattern formation in inclined layer convection, Phys. Rev. Lett. 84 (2000) 5320–5323.
[4] K.E. Daniels, E. Bodenschatz, Defect turbulence in inclined layer convection, Phys. Rev. Lett. 88 (2002) 034501.
[5] F.H. Busse, R.M. Clever, Three-dimensional convection in an inclined layer heated from below, J. Eng. Math. 26 (1992) 1–19.
[6] L. Prandtl, Essentials of Fluid Dynamics, Blackie, London, 1952.
[7] R.B. Stull, An Introduction to Boundary Layer Meteorology, Kluwer Academic Publishers, 1989.
[8] A.E. Gill, A. Davey, Instabilities of a buoyancy driven system, J. Fluid Mech. 35 (1969) 775–798.
[9] P.A. Iyer, Instabilities in buoyancy-driven boundary-layer flows in a stably stratified medium, Boundary-Layer Meteorology 5 (1973) 53–66.
[10] J.W. Elder, Laminar free convection in a vertical slot, J. Fluid Mech. 23 (1965) 77–98.
[11] A.E. Gill, Boundary-layer regime for convection in a rectangular cavity, J. Fluid Mech. 26 (1966) 515–536.
[12] B. Gebhart, Y. Jaluria, R.L. Mahajan, B. Samumakia, Buoyancy Induced Flows and Transport, Hemisphere, 1993.
[13] G. Desrayaud, Stability of flow near a heat-flux plate and comparison with numerical simulations in a square cavity, CNAM Report, 1990, 1990/LT/01.
[14] J. Tao, P. Le Quéré, S. Xin, Absolute and convective instabilities of natural convection flow in boundary-layer regime, Phys. Rev. E 70 (2004) 066311.
[15] G.D. McBain, S.W. Armfield, G. Desrayaud, Instability of the buoyancy layer on an evenly heated vertical wall, J. Fluid Mech. 587 (2007) 453–469.
[16] P.J. Schmid, D.S. Henningson, Stability and Transition in Shear Flows, Springer, 2001.